Supplementary information

1 Comparison against another parcel model with condensation process

The details of the numerical model used in Ghan et al. (2011) can be found in Abdul-Razzak et al. (1998) describing the condensation process in an air parcel rising adiabatically at uniform speed. For comparison here, the DCPM is tested with a constant updraft velocity ($dV/dt = 0$, see Eq. 3 in Sect. 2.1) and both collision-coalescence and entrainment ($\mu = 0$) processes excluded. Hence, the condensation process determines activated particle numbers and corresponding maximum supersaturation in both numerical models. We also applied the same initial conditions and the same baseline case with a single lognormal aerosol distribution, as specified in Ghan et al. (2011). The number fraction activated is defined as the fraction of particles with wet sizes larger than their critical values (Nenes et al., 2001) when maximum supersaturation is achieved. Figs. S1–S6 demonstrate that the simulated maximum supersaturation and number fraction activated from the DCPM are in good agreement with the numerical solutions in Ghan et al. (2011) for a wide range of updraft velocities, aerosol number concentrations, geometric mean radii, geometric standard deviations, hygroscopicity, and condensation coefficients. As discussed in Sect. 4.2.1, collision-coalescence of cloud droplets is ineffective at early stages of the observed cloud due to small drop sizes developed and the condensation process dominates droplet growth in the 12 June case-study. Therefore, we can conclude that this comparison supports the validity of the present model and justify the findings from its application to the IPHEx case-study.

2 Details of the WRF model configuration

A 5-day simulation (see the WRF domain configuration in Fig. 10a) over the SAM was performed using the advanced WRF model in version 3.5.1 (Skamarock et al., 2008) from 00:00 UTC 08 June for the first domain (06:00 UTC for second, third, and fourth domains) to 00:00 UTC 13 June 2014 for all four domains. The simulation was set up in a manner similar to Wilson and Barros (2015) and Sun and Barros (2012). One-way nested domains are configured with horizontal grid spacing of 15-, 5-, 1.25-, 0.25-km. This corresponds to grid sizes of 147×121, 267×288, 552×552, and 555×555 for the first (D01), second (D02), third (D03), and fourth (D04) domains, respectively. A terrain-following vertical grid with 90 layers is constructed with 30 levels in the lowest 1 km AGL and the model top is at 50 hPa. Initialization and lateral boundary conditions are updated every 6-hour using the National Centers for Environmental Prediction (NCEP) Final Operational Global Analysis (FNL) with 1°×1° horizontal resolution (Kalnay et al., 1996). The Kain-Fritsch cumulus parameterization scheme (Kain, 2004) is used in the D01 (15 km) and D02 (5 km) domains, and convection is resolved explicitly in the D03 (1.25 km) and D04 (0.25 km) domains. Other physics options include the Thompson cloud microphysics scheme (Thompson et al., 2008), a new version of the Rapid Radiative Transfer Model radiation scheme for longwave and shortwave (Iacono et al., 2008), and the unified

Noah land-surface model (Tewari et al., 2004) used for all four domains. The Mellor-Yamada-Janjic planetary boundary layer scheme (Janjic, 1994) is selected together with the Monin-Obukhov (Janjic Eta) surface layer scheme. The soil temperature and moisture fields are also initialized from the NCEP FNL data.

References

Abdul-Razzak, H., Ghan, S. J., and Rivera-Carpio, C.: A parameterization of aerosol activation: 1. Single aerosol type, Journal of Geophysical Research: Atmospheres, 103, 6123-6131, 10.1029/97jd03735, 1998.

Ghan, S. J., Abdul-Razzak, H., Nenes, A., Ming, Y., Liu, X., Ovchinnikov, M., Shipway, B., Meskhidze, N., Xu, J., and Shi, X.: Droplet nucleation: Physically-based parameterizations and comparative evaluation, Journal of Advances in Modeling Earth Systems, 3, 10.1029/2011ms000074, 2011.

Iacono, M. J., Delamere, J. S., Mlawer, E. J., Shephard, M. W., Clough, S. A., and Collins, W. D.: Radiative forcing by long-lived greenhouse gases: Calculations with the AER radiative transfer models, Journal of Geophysical Research, 113, 10.1029/2008jd009944, 2008.

Janjic, Z. I.: The step-mountain eta coordinate model: Further developments of the convection, viscous sublayer, and turbulence closure schemes, Monthly Weather Review, 122, 927-945, 1994.

Kain, J. S.: The Kain–Fritsch convective parameterization: an update, J. Appl. Meteorol., 43, 170–181, 2004.

Kalnay, E., Kanamitsu, M., Kistler, R., Collins, W., Deaven, D., Gandin, L., Iredell, M., Saha, S., White, G., Woollen, J., Zhu, Y., Leetmaa, A., Reynolds, R., Chelliah, M., Ebisuzaki, W., Higgins, W., Janowiak, J., Mo, K. C., Ropelewski, C., Wang, J., Jenne, R., and Joseph, D.: The NCEP/NCAR 40-year reanalysis project, Bull. Am. Meteorol. Soc., 77, 437–471, 1996.

Nenes, A., Ghan, S., Abdul-Razzak, H., Chuang, P. Y., and Seinfeld, J. H.: Kinetic limitations on cloud droplet formation and impact on cloud albedo, Tellus B, 53, 133-149, 2001.

Skamarock, W. C., Klemp, J. B., Dudhia, J., Gill, D. O., Barker, D. M., Wang, W., and Powers, J. G.: A description of the advanced research WRF version 3. Report TN-475+STR, National Center For Atmospheric Research, Boulder CO, 2008.

Sun, X., and Barros, A. P.: The Impact of Forcing Datasets on the High-Resolution Simulation of Tropical Storm Ivan (2004) in the Southern Appalachians, Monthly Weather Review, 140, 3300-3326, 10.1175/mwr-d-11-00345.1, 2012.

Tewari, M., Chen, F., Wang, W., Dudhia, J., LeMone, M. A., Mitchell, K., Ek, M., Gayno, G., Wegiel, J., and Cuenca, R. H.: Implementation and verification of the unified NOAH land surface model in the WRF model, In 20th conference on weather analysis and forecasting/16th conference on numerical weather prediction, pp. 11-15, 2004.

Thompson, G., Field, P. R., Rasmussen, R. M., and Hall, W. D.: Explicit Forecasts of Winter Precipitation Using an Improved Bulk Microphysics Scheme. Part II: Implementation of a New Snow Parameterization, Monthly Weather Review, 136, 5095-5115, 10.1175/2008mwr2387.1, 2008.

Wilson, A. M., and Barros, A. P.: Landform controls on low level moisture convergence and the diurnal cycle of warm season orographic rainfall in the Southern Appalachians, Journal of Hydrology, 531, 475-493, 10.1016/j.jhydrol.2015.10.068, 2015.

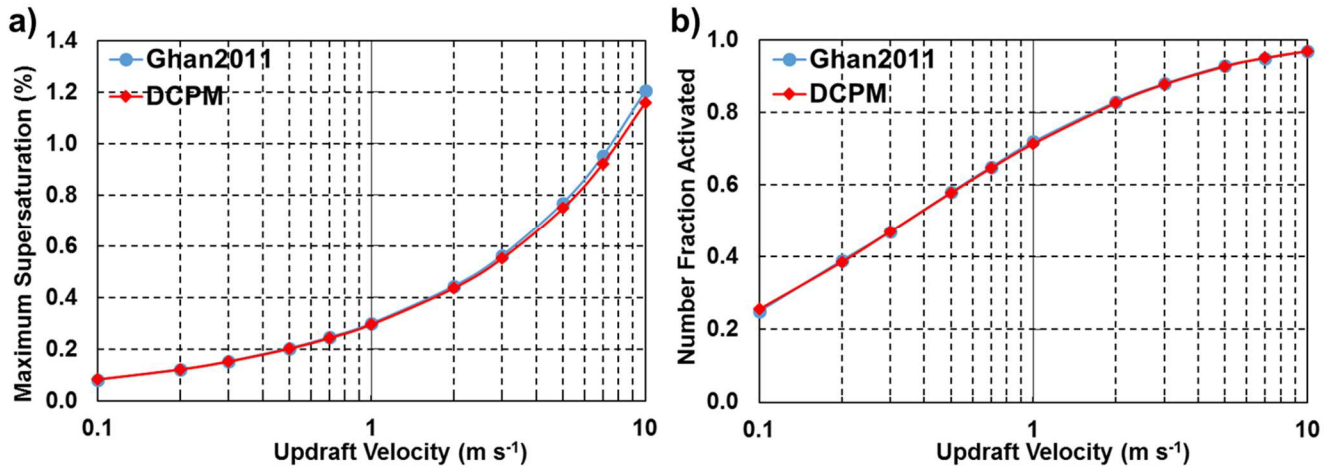

Figure S1: Maximum supersaturation (a) and number fraction activated as a function of updraft velocity calculated by the DCPM (red lines) compared to the numerical solution in Ghan et al., (2011; blue lines) using the same initial conditions and aerosol properties. In the baseline case, the aerosols have number concentration of 1000 cm^{-3}, geometric mean radius of 0.05 µm, a geometric standard deviation of 2, and a hygroscopicity of 0.7; the condensation coefficient is 1.0 and the uniform updraft is 0.5 m s^{-1}.

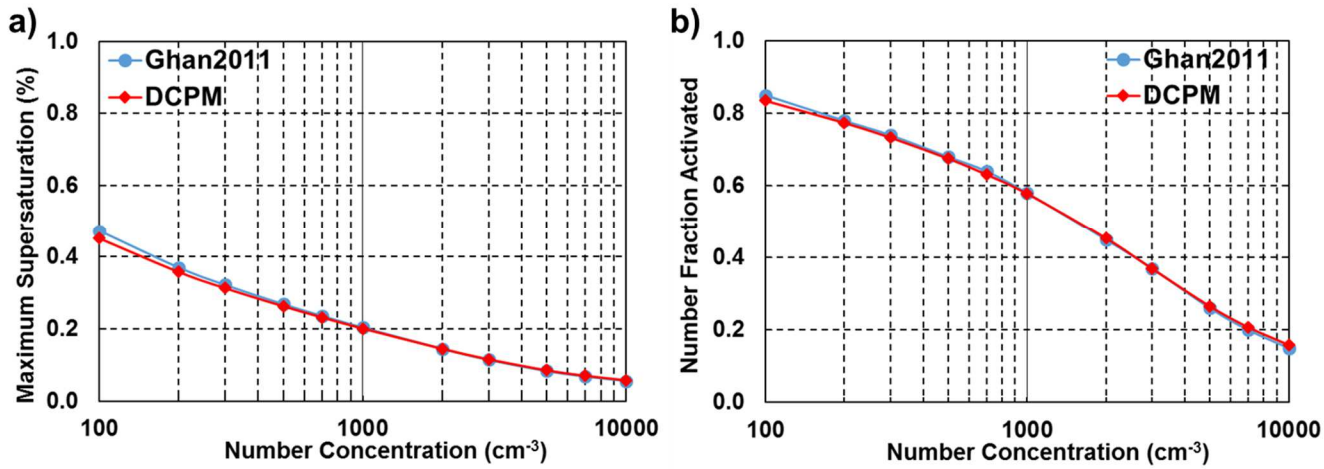

Figure S2: As in Fig. S1 but as a function of aerosol number concentration.

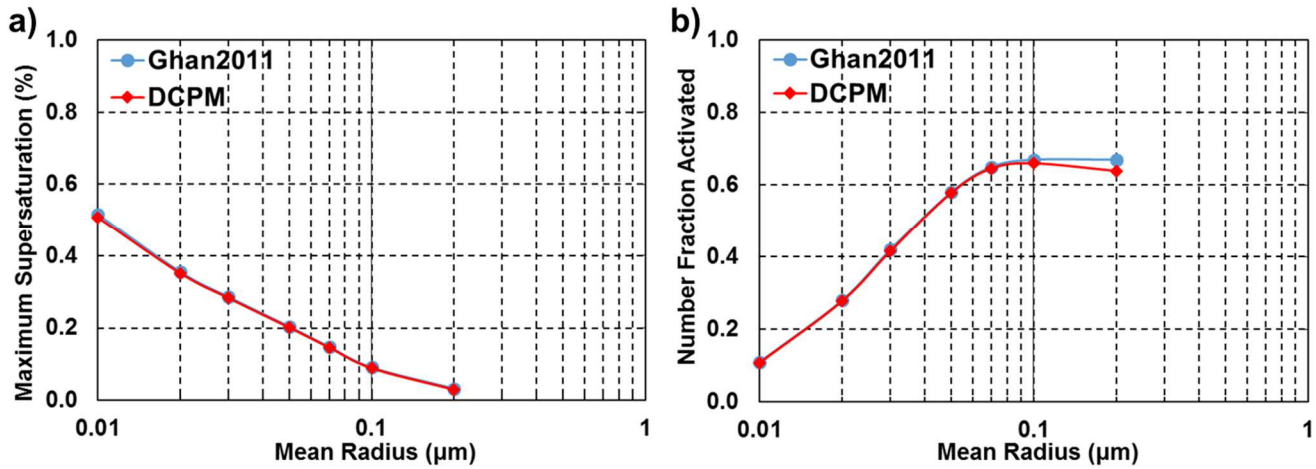

Figure S3: As in Fig. S1 but as a function of geometric mean radius of the single lognormal aerosol distribution.

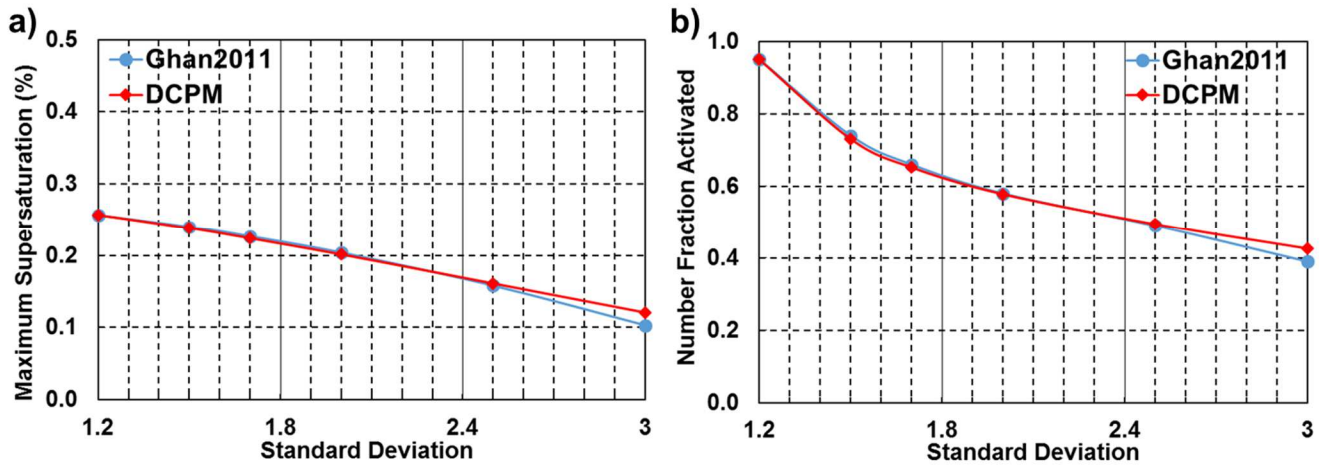

Figure S4: As in Fig. S1 but as a function of geometric standard deviation of the single lognormal aerosol distribution.

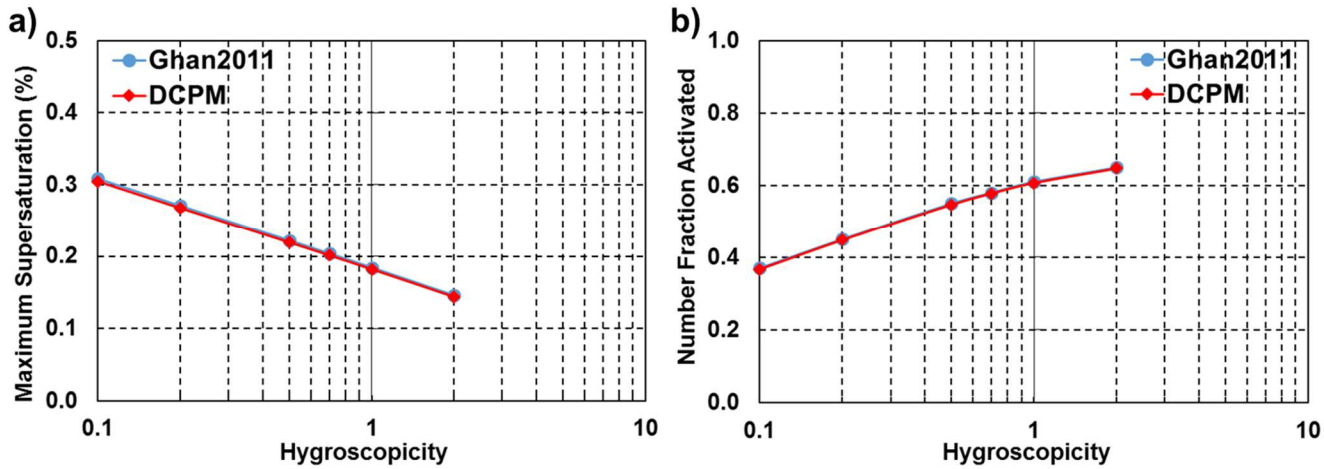

Figure S5: As in Fig. S1 but as a function of hygroscopicity.

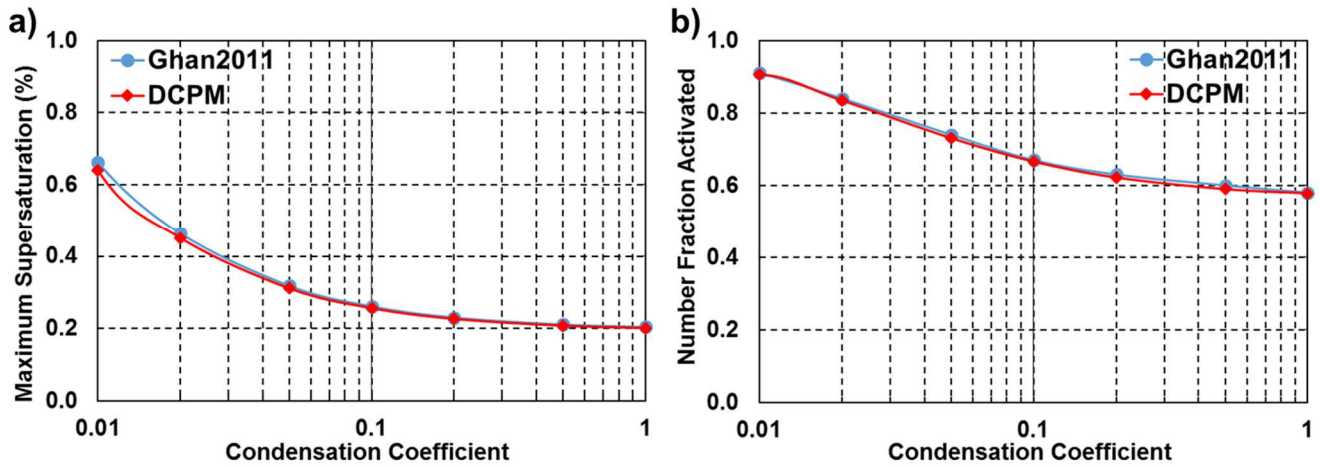

Figure S6: As in Fig. S1 but as a function of condensation coefficient.

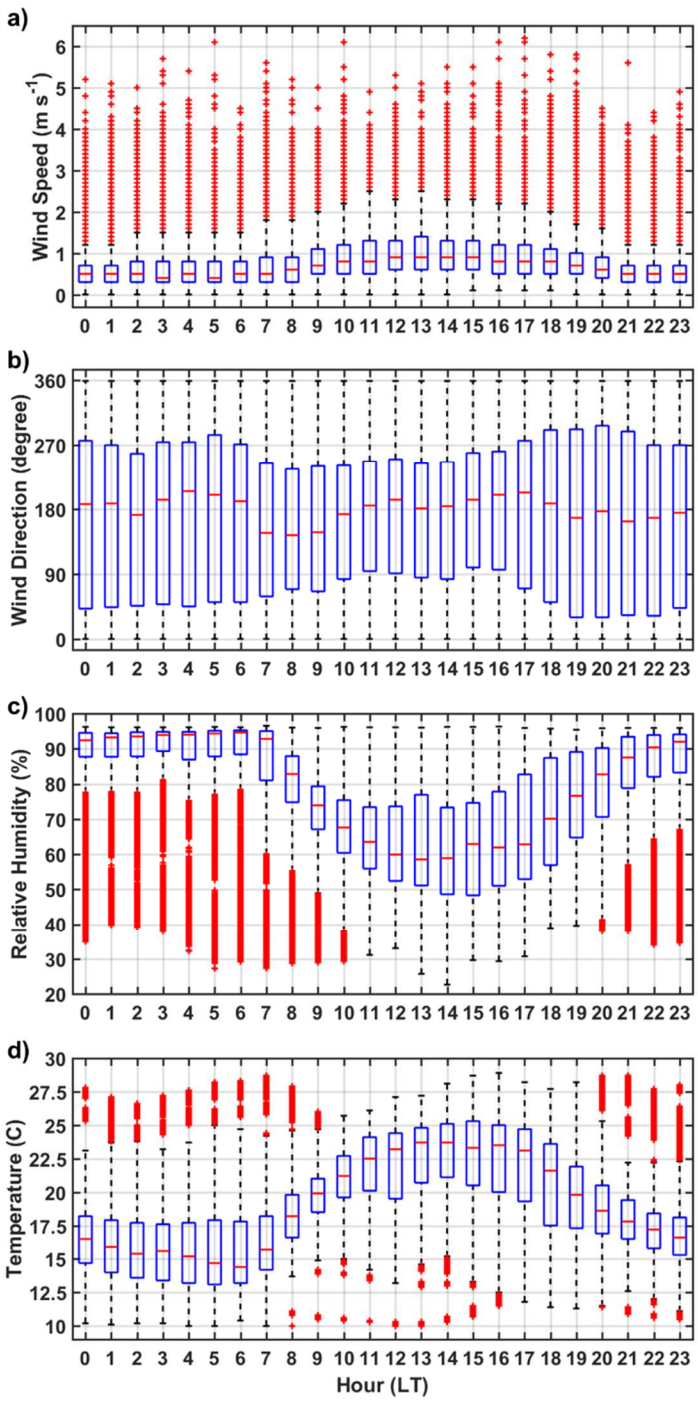

Figure S7: Diurnal cycles in local meteorological variables: wind speed (a), wind direction (b), relative humidity (c), and ambient temperature (d), measured at MV during the IPHEx IOP. The blue box represents the interquartile range (IQR) from the lower quartile (25th) to the upper quartile (75th), and the red short horizontal line inside the box indicates the median. The two horizontal black lines ("whiskers") extending from the central box denote the ±1.5 IQR interval, and red plus signs mark outliers that fall out of ± 1.5 IQR.

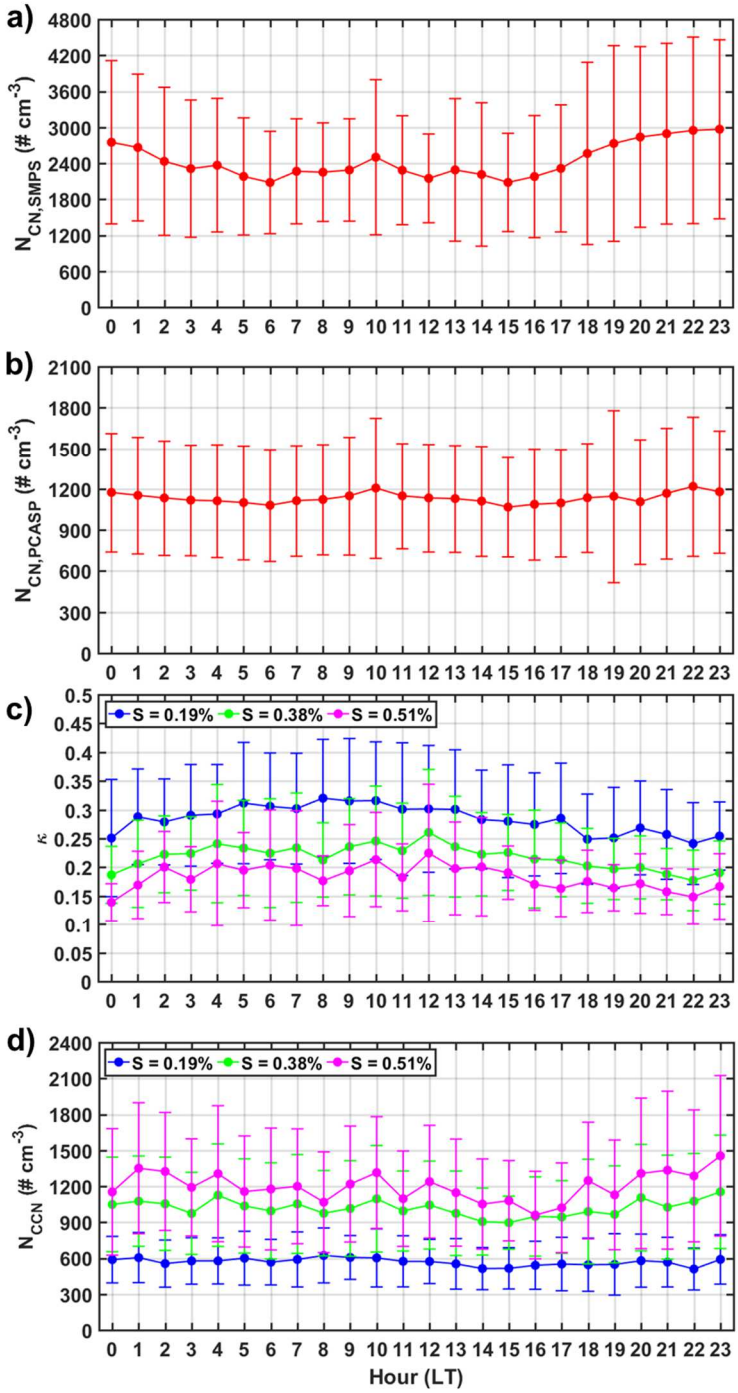

Figure S8: Diurnal cycles in total aerosol number concentrations from the SMPS ($N_{CN,SMPS}$, a) and PCASP ($N_{CN,PCASP}$, b), and in hygroscopicity parameter (κ, c) and CCN concentration (N_{CCN}, d) at three supersaturation (S) levels measured at MV during the IPHEx IOP. Mean values are denoted as solid circles and sample variability is indicated by short vertical bars, representing plus and minus one standard deviation.

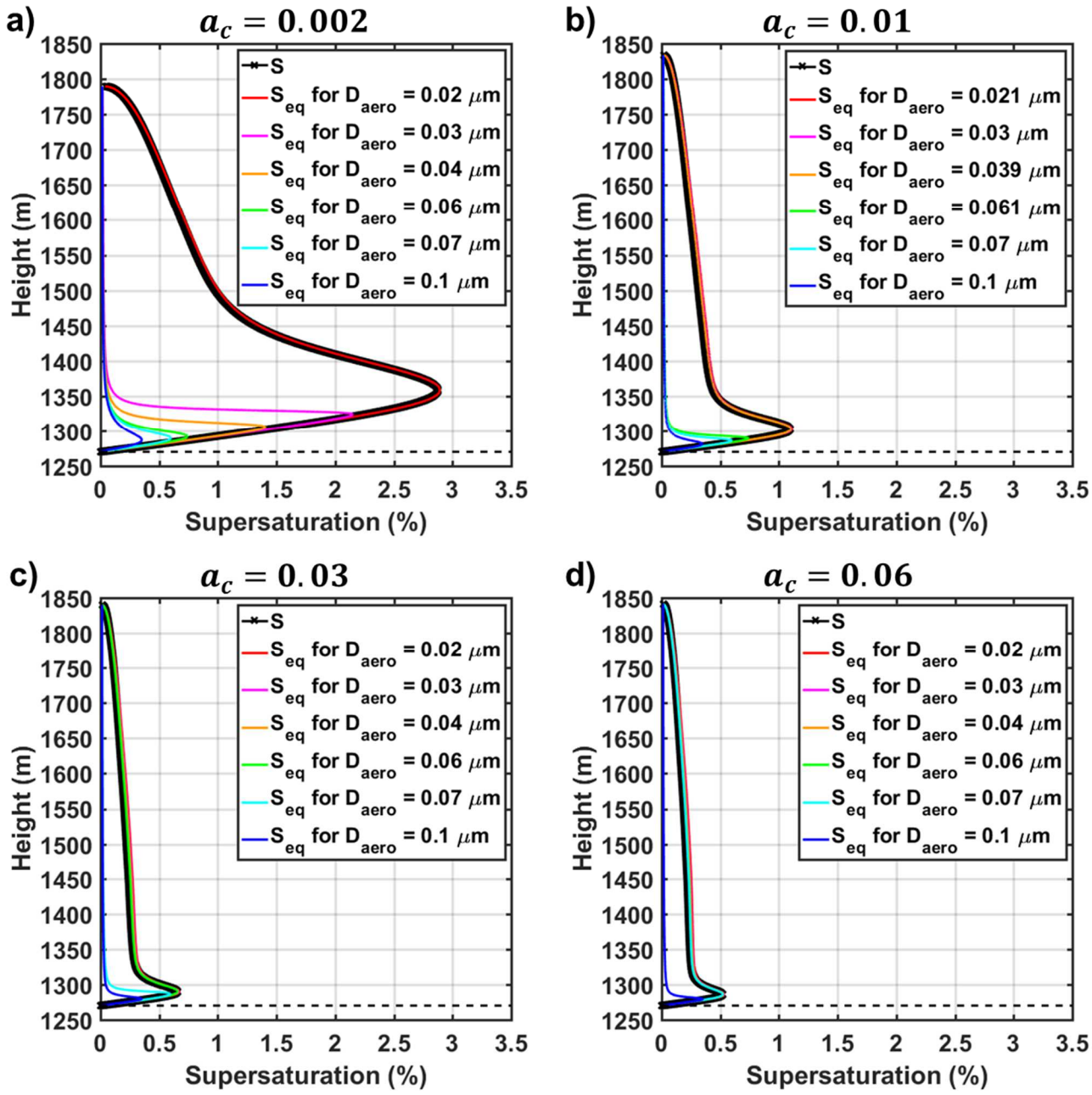

Figure S9: Variations with height of the parcel supersaturation (S, black lines) and droplet equilibrium supersaturation (S_{eq}, coloured lines) for six representative diameters of dry aerosol particles (D_{aero}) for four simulations: a) a_c = 0.002, b) a_c = 0.01, c) a_c = 0.03, and d) a_c = 0.06. The horizontal dashed line depicts CBH.